

Transport Theory and Correlation Measurements: Coming to Terms on Emission Sources

Pierre Nzabanimana^{1,2}, Pawel Danielewicz², and Giuseppe Verde³

¹*Los Alamos National Laboratory, Los Alamos, NM 87545*

²*Facility of Rare Isotope Beams and Department of Physics and Astronomy,
Michigan State University, East Lansing, Michigan 48824, USA and*

³*Istituto Nazionale di Fisica Nucleare, Catania, Sicily, Italy*

Two-particle correlations play a pivotal role in understanding the space-time characteristics of particle emission in Heavy-ion collisions. These characteristics are typically represented by a relative emission source and can be obtained using transport model simulations such as the Boltzmann-Uehling-Uhlenbeck (BUU) transport model. In this paper, we utilize the BUU transport model to simulate the p-p source. Subsequently, we integrate this source and the p-p kernel within the KP formula to calculate the correlations. By comparing the correlations obtained from the BUU simulation with those obtained using imaging methods, such as the deblurring method, we aim to gain a deeper understanding of the impact of fast and slow emissions on the measured correlations. Specifically, this comparison is used as a tool to determine a function (tail) that represents the relative distribution of the particle pair from secondary decay emissions. Thus, we correct the BUU source function by incorporating a tail to account for the contribution of secondary decay emissions, which cannot be accurately captured by BUU simulations. Resulting source function reproduces the features in the measured correlations. To illustrate our approach, we examine p-p correlations measured in Ar + Sc reactions at $E/A = 80$ MeV, considering both momentum-independent and momentum-dependent nuclear equations of state (EOS).

I. INTRODUCTION

Transport models are used to extract information about the nuclear Equation of State (EoS) (see [1] and Refs. therein) from heavy-ion collision data. Results from extensive studies performed with the Boltzmann-Uehling-Uhlenbeck model (BUU), the Quantum Molecular Dynamics model (QMD), and the Antisymmetrized Molecular Dynamics Model (AMD) can be found in the literature [1–3]. These models solve nuclear transport equations governed by interaction terms connected to the EoS. The results of their simulations are compared with those of experimentally measured observables to infer the EoS and other transport properties used as input parameters. More recently, the study of the N/Z-asymmetry dependence of the EoS has become increasingly important because of their potential implications on the interior of neutron stars (see [4] and Refs. therein). The accelerator facilities providing beams with ranges of neutron-proton asymmetries and transport simulations have therefore provided tools to study nuclear matter of astrophysical relevance under laboratory-controlled conditions.

Understanding the complex dynamics of heavy-ion collisions calls, in particular, for a theoretical and experimental treatment of observables that test the space-time features of the collision process. Particle-particle correlations have been extensively used [5, 6], and the mentioned transport theory provides a framework for understanding what they may reveal. In this manuscript, we use the pBUU transport approach, developed by Danielewicz and Bertsch [7], describing the time evolution of a single-particle phase-space distribution and nucleon-nucleon collisions [1, 5, 8]. Particles follow classical trajectories under the influence of a mean-field poten-

tial and nucleon-nucleon collisions. The phenomenological at its root model requires several parameters for the scattering cross-section and mean field, and elementary data, heavy-ion collision data, and theoretical considerations constrain their variability range, with EoS implications.

The quantity linking pBUU and other BUU models [5, 9] with the correlation data is the so-called two-particle source function $S(r)$, that is the probability density of emitting a pair of particles, usually protons, at a relative distance r at the time when the second particle is emitted. Following the so-called Koonin-Pratt equation [10–12], one can fold the square of a final-state wave function calculated theoretically with the source from transport to arrive at a correlation function to be compared with the data.

Since BUU involves several adjustable parameters, one can likely learn correlation function data by comparing the source function obtained from BUU with the one obtained from imaging methods [6]. Recently, a new imaging approach called "deblurring" has been introduced in Refs. [13–15]. The parameters yielding the source function better conforming with the outcomes of imaging and deblurring approaches can be used to constrain the nuclear equation of state (EoS) and other important transport properties. In particular in Ref. [5], the source function calculated with BUU simulations was compared to the sources imaged from experimental correlation functions. The two-proton correlation was found to be sensitive to the details of the in-medium nucleon-nucleon cross-section, σ_{NN} . Moreover, in Ref. [16], a transport model was used to study the effects of the density dependence of the nuclear symmetry energy on two-nucleon (pp, np and nn) correlations in heavy-ion collisions. In-

deed, the density dependence of the nuclear symmetry energy affects nucleon emission times at the early stage of the collision and, consequently, the space-time extent of their emitting sources. The conclusions of the article point to the possibility of using two-nucleon correlations as a tool to probe the symmetry energy. A similar analysis with the same model showed that including momentum-dependent interactions may reduce the sensitivity of two-nucleon correlations to the density dependence of the symmetry energy [16]. A quantitative pursuit of the symmetry energy with correlations thus requires the study of multiple observables that can also constrain the details of momentum-dependent interactions.

To learn about the two-particle emitting source function from correlations, one needs to solve the Koonin-Pratt (KP) equation [10–12],

$$C(\mathbf{q}) = \int d^3r K(\mathbf{q}, \mathbf{r}) S(\mathbf{r}). \quad (1)$$

In this equation, the correlation function, $C(\mathbf{q})$, is expressed as a function of the relative momentum of the two particles, $\mathbf{q} = (\mathbf{p}_1 - \mathbf{p}_2)/2$, with the momentum vectors of \mathbf{p}_1 and \mathbf{p}_2 of the two particles in the center of mass. The right-hand side of the equation contains the integral over relative distance of the product between the kernel function $K(\mathbf{q}, \mathbf{r})$ and the source function $S(\mathbf{r})$, namely the probability density of the pair emitted at relative distance \mathbf{r} . In the equation, the relative distance \mathbf{r} is calculated when the second particle is emitted [10, 11, 17]. The kernel is the square modulus of the pair relative wave function with the outgoing boundary condition of the relative momentum \mathbf{q} determined at the detectors. For details on how the KP formula can be derived, we suggest Ref. [18].

In the literature, the source functions have typically been parameterized as Gaussian functions due to the simplicity of the form [19]. Then, the best fits of Eq. 1 to the measured correlation functions provide access to the width of the Gaussian source, left as an adjustable parameter [6, 11, 20–22]. Most of the literature has used angle-averaged correlation functions, where the above KP equation is integrated over all directions between relative momentum and relative distance, \mathbf{q} and \mathbf{r} , respectively.

In this paper, we study two-proton angle-averaged source functions extracted from pBUU simulations of $^{36}\text{Ar}+^{45}\text{Sc}$ collisions at $E/A=80$ MeV, using different choices of symmetry matter EoS parameters (stiff and soft) and both momentum-dependent and independent interactions. In the rest of the paper, unless otherwise specified, we use EoS to refer to the symmetric matter EoS. These pBUU source functions are then compared with source profiles extracted from experimentally measured two-proton correlation functions, analyzed with the *deblurring method*, which was demonstrated in tests to return input sources [14]. This method represents a step forward in studying correlations without a priori

assumptions about the Gaussian functional form of the emitting source function [14, 23, 24]. The experimental data were collected at the National Superconducting Cyclotron Laboratory (NSCL) at Michigan State University [25].

The performed pBUU simulation does not include secondary decay and long-lived emission processes that mainly contribute to the shape of the source function at large r -values, where the Coulomb repulsion dominates the final-state interactions of proton pairs. These pairs of protons contribute to the shape of the correlation function at small values of q , $q < 10$ MeV / c , where anticorrelation is observed. To account for this critical contribution to the data analysis, we add an exponential decay parameterization of the long-lived emitting source to the dynamic source obtained from pBUU simulations. The free parameters of this second exponential source are determined by comparing the theoretical source with the source function obtained by deblurring the experimental data.

The manuscript is organized as follows. Section II discusses pBUU transport model simulations. The theoretical sources and correlations of two protons are discussed in section III. The sources obtained from the deblurring of data and their comparison to the model are presented in section IV. Then, the pBUU study of the two-proton emitting source results are discussed in section V. We summarize the results of our work in section VI.

II. BUU MODEL

The BUU model is a semi-classical one-body transport model extensively used to describe the dynamics of heavy-ion collisions at intermediate energies. In this model, all one-body observables for a system are determined by single-particle phase-space densities $f = f(\mathbf{p}, \mathbf{r}, t)$ that evolve self-consistently with time. We use the pBUU code to solve the Boltzmann equations for f [2, 26],

$$\left(\frac{\partial}{\partial t} + \mathbf{v}_\mathbf{p} \cdot \nabla_\mathbf{r} - \nabla_\mathbf{r} U(\mathbf{r}) \cdot \nabla_\mathbf{p} \right) f = I_{col}(\sigma_{in}, f). \quad (2)$$

The left-hand side of Eq. (2) accounts for the motion of the particle at velocity $\mathbf{v}_\mathbf{p} = \nabla_\mathbf{p} \epsilon$ subject to force $-\nabla_\mathbf{r} U(\mathbf{r})$. Here, m , \mathbf{p} , and ϵ are the mass, momentum, and single-particle energy, respectively. On the right-hand side, I_{ol} is the collision term that accounts for nucleon-nucleon collisions

$$I_{col} = \frac{g}{h^3} \int d^3\mathbf{p}_2 \int d\Omega \frac{d\sigma_{12}}{d\Omega} v_{12} * [\hat{f}_1 \hat{f}_2 \hat{f}_{1'} \hat{f}_{2'} - f_1 f_2 \hat{f}_{1'} \hat{f}_{2'}], \quad (3)$$

where $f_{i=1,2}$ is single particle phase-space distribution, \hat{f} is the statistical factor equal to $1 - f$ for Fermi-Dirac statistics, $g = 2$ is spin degeneracy, and $\frac{d\sigma_{12}}{d\Omega}$ is differential cross section for scattering to angle Ω . The primed

indices pertain to the final momenta and the initial momenta are \mathbf{p}_1 and \mathbf{p}_2 and correspond to relative velocity v_{12} , the relative momentum is $\mathbf{q}_{12} = \mu(\mathbf{v}_1 - \mathbf{v}_2)$, where μ is the reduced mass, reducing to $\mathbf{q}_{12} = \mathbf{p}_1 - \mathbf{p}_2$ for identical masses. The total momentum is $\mathbf{P}_{12} = \mathbf{p}_1 + \mathbf{p}_2$. The final relative momentum is determined by the scattering angle, $\Omega = (\theta, \phi)$ so that the final relative momentum is $q_{1'2'} = q_{12} (\sin \theta \cos \phi, \sin \theta \sin \phi, \cos \theta)$. Notably, for the elastic collision, the total momentum remains constant while the final and initial relative momenta are equal in magnitude (i.e., $q_{12} = q_{1'2'}$, hence $\mathbf{q}_{1'2'}$ is determined by scattering angle).

The BUU model is a complex and requires a number of input parameters, such as EoS and the mean-field potential (including the symmetry energy and mean-field momentum dependence needed both in the Boltzmann and TF equations) and the in-medium nucleon-nucleon collision cross-sections (with their energy and density dependence), to list a few. When initializing a collision, we need to set the impact parameter that significantly affects the dynamics. We use the parameters corresponding to incompressibility, $K=214$ MeV and 280 MeV, for softer and stiffer EoS, respectively. In addition, when the momentum-dependent potential is switched on in pBUU, the effective mass $m^* = 0.7m$ is used, where $m^* = \frac{p^F}{v^F}$, with p^F and v^F representing the Fermi momentum and velocity, respectively, and m being the nucleon mass [2].

In the mean-field potential, the interaction symmetry energy we use has a density dependence, $\mathcal{S}_{pot}(\rho) = \mathcal{S}_0(\rho/\rho_0)^\gamma$, where $\rho_0 = 0.16 \text{ fm}^{-3}$ is the saturation density of nuclear matter. The exponent γ defines the stiffness of the density dependence of the symmetry energy. Typically, $\gamma < 1$ corresponds to a soft symmetry energy, while $\gamma \geq 1$ corresponds to a stiff symmetry energy, with \mathcal{S}_0 being a fixed parameter. When the momentum-dependent potential is switched on, we use $\gamma = 0.5$ for a soft EoS and $\gamma = 1.6$ for a stiff EoS. All the different parameters in the model affect the observables that can be measured experimentally.

The initial densities for the colliding nuclei are determined within the Thomas-Fermi (TF) approximation for the systems, specifically following the equations:

$$\begin{aligned} \tilde{\epsilon}_n^F - a_1 \nabla^2 \left(\frac{\rho}{\rho_0} \right) + \delta^2 \rho^2 \frac{d}{d\rho} \frac{\mathcal{S}_{pot}}{\rho} \\ + 2\delta \rho \mathcal{S}_{pot} - \mu_n = 0, \end{aligned} \quad (4)$$

$$\begin{aligned} \tilde{\epsilon}_p^F - a_1 \nabla^2 \left(\frac{\rho}{\rho_0} \right) + \delta^2 \rho^2 \frac{d}{d\rho} \frac{\mathcal{S}_{pot}}{\rho} \\ - 2\delta \rho \mathcal{S}_{pot} + U_{Coul} - \mu_p = 0. \end{aligned} \quad (5)$$

The TF equations are obtained by requiring that the energy is at a minimum in the ground state of the nucleus with a definite number of protons and neutrons. Here, $\rho = \rho_n + \rho_p$ is net nucleon density and $\delta = (\rho_n - \rho_p)/\rho$ is local relative neutron-proton asymmetry. In addition, U_{Coul} is the local Coulomb potential and a_1 is a parameter that controls the diffuseness of the surface, tied to

the surface energy [2]. With i referring to particle species, μ_i is the chemical potential of the species and $\tilde{\epsilon}_i^F$ is the Fermi energy computed without symmetry energy and Coulomb contributions.

The TF equations are solved employing the boundary condition of neutron and proton densities: $\rho_{n,p}(r \rightarrow \infty) = 0$ and $\frac{d\rho_{n,p}}{dr}|_{r=0} = 0$. These equations are numerically solved, starting with the initial values of $\rho_{n,p}$ and iteratively adjusting the chemical potentials [26]. The phase-space distribution functions f in the transport equations are represented by a large number of test particles. Those particles are distributed uniformly within the Fermi spheres corresponding to the local densities in the nuclei.

Previously, in Ref. [5], it was reported that the shape of the two-proton source function is significantly affected by the in-medium nucleon-nucleon collision cross-section, σ_{NN} . With a simplified approach, aimed at explaining the reasons behind such a sensitivity, the size of the source function exhibits the scaling $R \propto \sqrt{\sigma_{NN} A}$ [5]. Furthermore, IBUU simulations of $^{52}\text{Ca} + ^{48}\text{Ca}$ central collisions have explored the sensitivity of proton-proton correlation functions to the stiffness of the density dependence of the symmetry energy (Ref. [16]). It must be underlined that this sensitivity to the \mathcal{S} has been observed to undergo a significant reduction when momentum-dependent interactions are used in the same model simulations [16] and mostly concerns neutron-proton correlation functions that are difficult to measure experimentally. However, the effect of the symmetry part of the mean-field potential on the emission times of protons is still a reasonable expectation that deserves further exploration with correlation function studies.

In this manuscript, we explore the effects of soft and stiff EoS on two-proton source functions, when both momentum-independent and momentum-dependent interactions are considered. Note that in pBUU, in the case of likely more realistic momentum-dependent interactions, as mentioned before, the mean-field part of the symmetry energy is also implemented.

To understand how different reaction stages may affect the emission sources explored, we analyzed the time evolution of the reaction for both softer and stiffer EoS. Figures 1 and 2 show the time dependence (from 0 to 80 fm/c) of the density contour plots for the collision system, $^{36}\text{Ar} + ^{45}\text{Sc}$ at 80 A MeV (at an impact parameter of $b = 1.9$ fm), within the reaction plane. Figure 1 corresponds to the softer EoS, while Figure 2 corresponds to the stiffer EoS. In addition, we study the effects induced by switching on (top panels in Figs. 1 and 2) and off (bottom panels in Fig. 1 and 2) the momentum dependence for both soft and stiff EoS, respectively.

As depicted in the figures, at a time equal to 40 fm/c, the two colliding nuclei form a compound system. At 80 fm/c, notable differences are observed between the momentum-dependent and momentum-independent EoSs, particularly for the stiff EoS. When momentum dependence is present, the colliding nuclei produce two

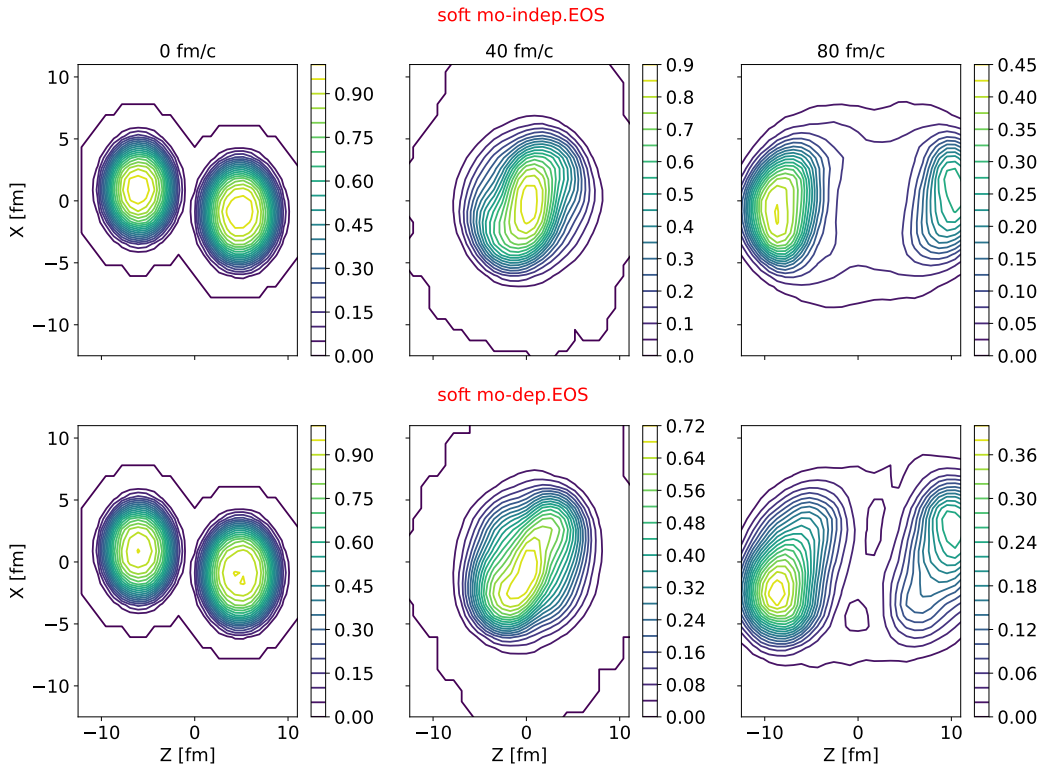


FIG. 1. Density contour plots for the reaction Ar + Sc at 80 MeV in the reaction plane, at widely spread times during the reaction. The first row shows the results for momentum-independent and the second row for momentum-dependent soft EoS. The side color bars provide transcription from the contour color to density values in units of normal density, ρ_0 .

excited fragments that fly apart in the final state. In contrast, the nuclear system exhibits a more elongated shape for the momentum-independent case, and the two fragments are not entirely separated at 80 fm/c. At that time, it is also evident from the contour plots that the nuclear system expands more (i.e., the materials in the system occupy more space) for soft EoS than for stiffer EoS. This is reflected in the density values of the plots for different contours, with color legends provided in the side vertical bars. Possibly related observations were made in Ref. [27]. Differences in expansion can influence particle emissions and, consequently, particle correlations. However, gaining deeper insight into this effect requires analyzing the time dependence of the emitting source function, which is beyond the scope of this paper but is being considered for our future work.

III. TWO-PROTON CORRELATION FUNCTIONS

Two-particle correlations can be experimentally measured in heavy-ion collisions as the ratio between two-

proton coincidence yields, $Y_{coinc}(\mathbf{p}_1, \mathbf{p}_2)$ and the product of single particle proton spectra, $Y(\mathbf{p}_1) \cdot Y(\mathbf{p}_2)$, where \mathbf{p}_1 and \mathbf{p}_2 are the momenta of the protons [19, 28]:

$$C(\mathbf{q}) \equiv 1 + R(\mathbf{q}) = c \frac{Y_{coinc}(\mathbf{p}_1, \mathbf{p}_2)}{Y(\mathbf{p}_1)Y(\mathbf{p}_2)}. \quad (6)$$

Here, c is a constant to be chosen such that $R(q) = 0$ at large q -values. In BUU, we can compute the two-particle source function, $S(r)$, from the phase-space distribution of protons, as they decouple from the colliding system [18]. The source function can then be used to calculate the correlation function using the KP equation (see Eq. 1) once the proton-proton kernel is calculated. In this section, we use this approach to explore the two-proton pBUU correlation functions calculated for central collisions $^{36}\text{Ar} + ^{45}\text{Sc}$ at 80 MeV per nucleon. Then we compare the sources of pBUU with those obtained from the deblurring method of [13, 14], applied to the experimental data of [5]. Furthermore, we test the effects induced by both the stiffness of EoS, including symmetry energy, and the momentum dependence on the shape of the source function.

In our simulations of the pBUU model, the p-p correlation function is calculated from [29]:

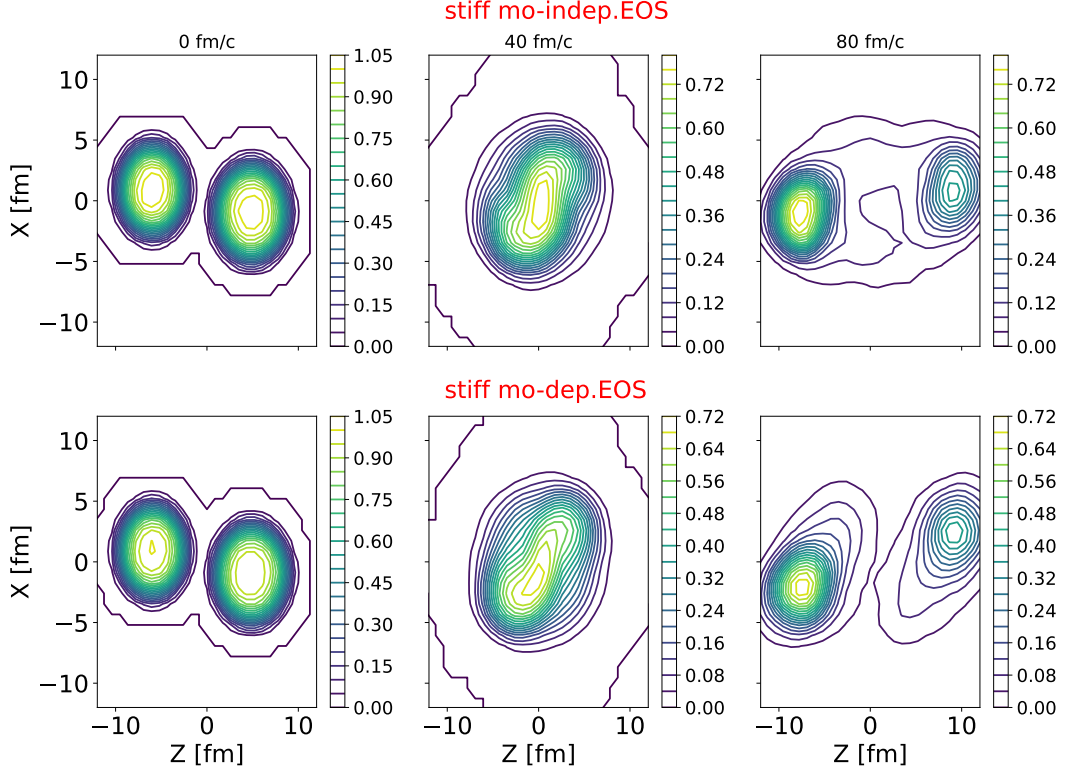


FIG. 2. Similar results to Fig. 1, but for the stiff EoS.

$$C(\mathbf{q}) \equiv 1 + R(\mathbf{q}) = \int d^3r |\Psi_{pp}(\mathbf{q}, \mathbf{r})|^2 \frac{\int d^3R f(\mathbf{P}/2, \mathbf{R} + \mathbf{r}/2, t') f(\mathbf{P}/2, \mathbf{R} - \mathbf{r}/2, t')}{(\int d^3r' f(\mathbf{P}/2, \mathbf{r}', t'))^2}. \quad (7)$$

Here,

$$S^{BUU}(\mathbf{r}) = \frac{\int d^3R f(\mathbf{P}/2, \mathbf{R} + \mathbf{r}/2, t') f(\mathbf{P}/2, \mathbf{R} - \mathbf{r}/2, t')}{(\int d^3r' f(\mathbf{P}/2, \mathbf{r}', t'))^2}, \quad (8)$$

can be identified as the source function calculated directly from the relative position $\mathbf{r} = \mathbf{r}_1 - \mathbf{r}_2$ and total momentum $\mathbf{P} = \mathbf{p}_1 + \mathbf{p}_2$ of the particles at the time when the last particle is emitted [5]. The center of mass position for equal mass particles is $\mathbf{R} = (\mathbf{r}_1 + \mathbf{r}_2)/2$. The phase space distribution f , which has already appeared in the Boltzmann equation (2), is now taken at time t' following particle emission. As such, it may be calculated by integrating out the rate g of emission of final particles:

$$f(\mathbf{p}, \mathbf{r}, t') = \int_{-\infty}^{t'} dt \cdot g(\mathbf{p}, \mathbf{r} - \mathbf{v}_p(t' - t), t). \quad (9)$$

This underscores the interplay between spatial and temporal emission features, illustrated in Fig. 3, that get folded out in the source function for correlation in (1). In particular, prolonged emission from a quasi-stationary subsystem can result in a significant anisotropy of both the source S and the correlation R [30]. In this work, we

shall concentrate on angle-averaged sources and correlations related by the angle-averaged kernel:

$$C(q) = 4\pi \int dr r^2 K(q, r) S(r). \quad (10)$$

The kernel calculations are described in several papers [12, 17, 31].

When focusing on particle emission, two stages can be distinguished in the evolution of collisions modeled in pBUU transport simulations. There is an early stage of fast nucleon emission (often referred to as the pre-equilibrium stage). That is followed by a more gradual emission stage where particles are emitted over increasingly longer timescales [6]. The pre-equilibrium stage, from a few fm/c after nuclei come into contact, makes a more substantial contribution to particles coming out at large transverse velocities, in a focused manner, with particles of similar velocity coming out at shorter timescales

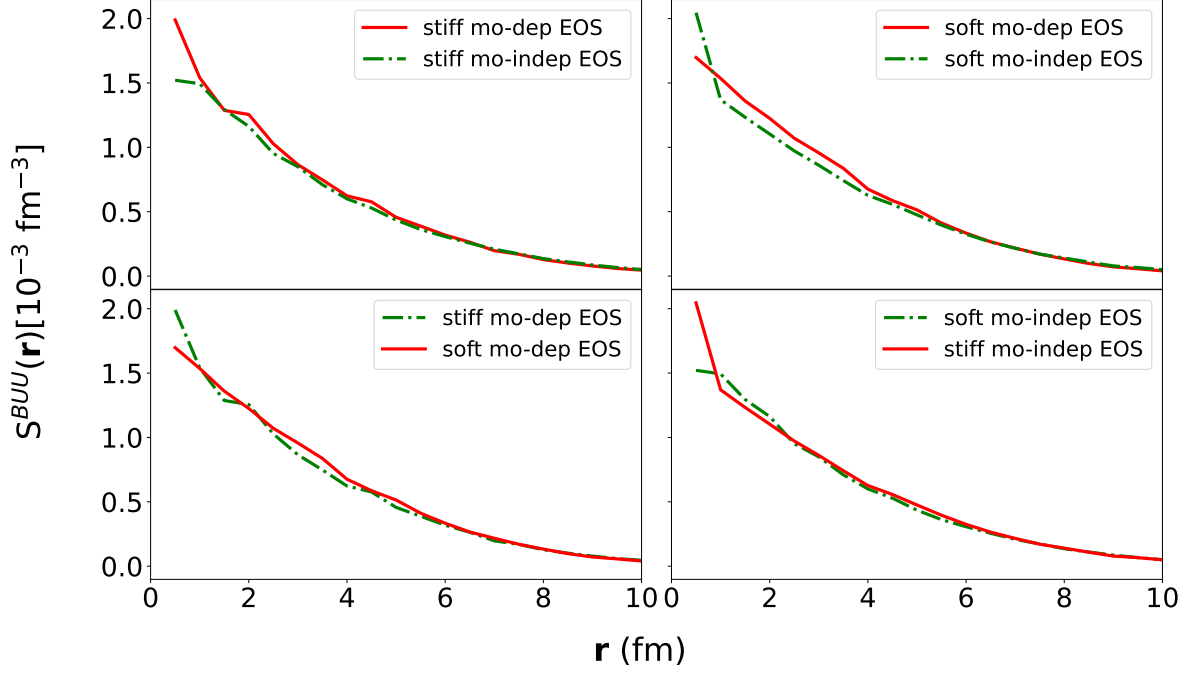


FIG. 3. Relative proton-proton source function, obtained from pBUU simulation of $^{36}\text{Ar} + ^{45}\text{Sc}$ collision at 80 MeV/nucleon and $b=1.9$ fm, shown as a function of relative position r , for 200-400 MeV/c cut in total pair momentum, following experiment [5]. The top panels compare results with and without momentum dependence in the energy functional, and the bottom panels compare results for different EoS stiffness.

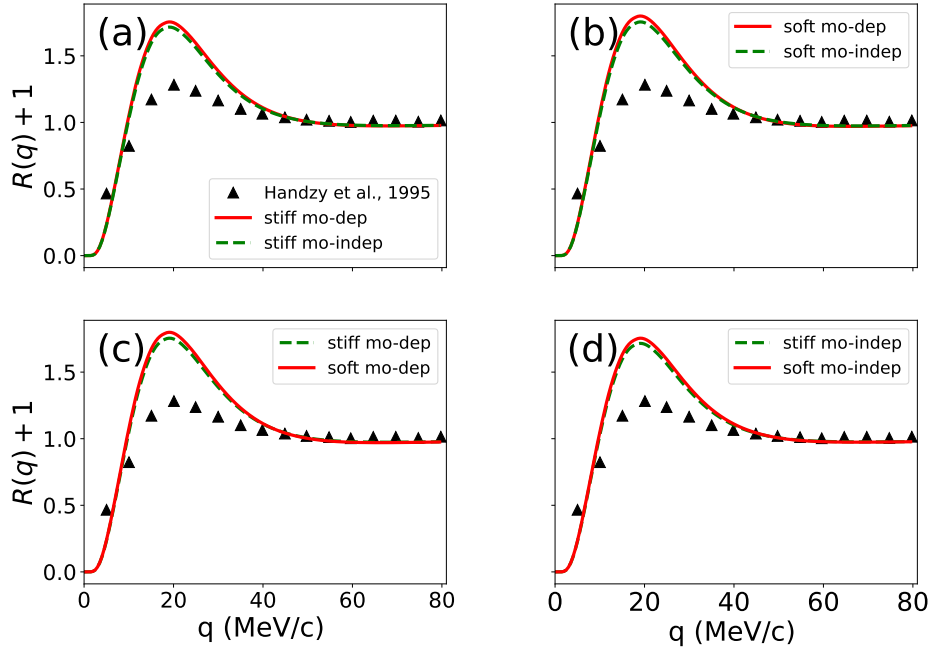


FIG. 4. $p - p$ correlation functions for $^{36}\text{Ar} + ^{45}\text{Sc}$ collisions at $E/A = 80$ MeV in the total momentum bracket $P = 200$ -400 MeV/c. The symbols represent data of Ref. [25] and the lines - pBUU calculations at $b = 1.9$ fm for various energy functionals. The top panels explore sensitivity to momentum dependence in the energy functional, and the bottom panels explore sensitivity to EoS stiffness.

and distances from each other. The follow-up slower emission phase makes a more substantial contribution to

particles coming out at lower transverse velocities, in a less focused manner. That phase further contributes one

or both members to the pairs at similar velocities, coming over a wider time spread and at large r from each other. Both emission stages contribute to the sources behind correlation functions, though to a different degree depending on the momentum region for the particles. At any momentum, the pre-equilibrium emission alone contributes more strongly to the short- r portion of S than long- r , and the late emission generally feeds large r [5].

The proton-proton pBUU sources calculated for the collision $^{36}\text{Ar} + ^{45}\text{Sc}$ at $E/A = 80$ MeV with $b=1.9$ fm, after experiment [5], following different versions of the functional pBUU energy, are shown in Fig. 3. The source profiles lack significant contributions past ~ 10 fm, regardless of the EoS. Notably, the large- r contributions to S are not optimally modeled in the Boltzmann equation-like approaches. Physically, at least one pair member within the pairs at large r is likely to stem from cascading decays of excited secondary fragments. Such decays are missing from approaches based on the Boltzmann equation (2). On the other hand, such approaches have a good chance of correctly describing the short- r shape of S , where both pair members are likely to arise from early emission, though not necessarily the overall strength of S there.

We use the source functions obtained from pBUU simulations as inputs to the angle-averaged Koonin-Pratt equation 10. The correlation functions obtained using different energy functionals are shown as lines on Fig. 4. The triangles represent experimental correlations obtained in the central reaction $^{36}\text{Ar} + ^{45}\text{Sc}$ at 80 MeV / A, with the proton pairs having total momenta $P = |\mathbf{p}_1 + \mathbf{p}_2|$ restricted to values between 200 and 400 MeV/c [5].

Qualitative features of the correlation functions in the calculations, and by inference in the data, reflect interplay among several factors, including the short-range attractive nuclear interaction, the antisymmetrization effect due to the fermionic nature of protons, and the long-range repulsive Coulomb interaction between the emitted protons. All these effects are accounted for in the kernel function. The attractive nuclear interaction gives rise to a resonance around $q = 20$ MeV/c reflected in the peak in the correlation function in Fig. 4. Details in the peak of the correlation function depend on the overlap of the resonance wave function squared with the short-distance portion of the source function [6]. The Coulomb repulsion depletes the wave function at moderate relative distances, with the depletion hole increasing in size as q decreases, generally following an increase in radius for the classical Coulomb barrier. In Fig. 4, the Coulomb repulsion yields an anticorrelation at $q < 10$ MeV/c. The details of the correlation fall-off depend on how much the source function extends past the Coulomb barrier for a given q . Notably, the low- q region is generally difficult to measure experimentally, as it is populated by proton pairs at small relative angles that accumulate in the same detection cell. Such experimental limitations will likely leave some long- r information on the source incomplete. On

the theoretical side, because of the probabilistic nature of the source S , which integrates over \mathbf{r} to 1, any uncertainties at large r impact the overall strength of S at short r , though not the shape there. As a counterpart, an analysis of the correlation at large q can provide information on the net fraction of pairs in S at large r , because of the normalization condition, as will be reminded below.

In Fig. 4, it can be observed that the momentum-dependent EoS tends to yield a slightly more prominent peak at 20 MeV/c for both the stiff and soft EoS cases. It also appears that the soft EoS exhibits a slightly higher peak than the stiff EoS at the peak position. Nevertheless, the impacts of the energy functional are minor compared to the overall discrepancy between the theory and the data.

The main difference observed between the simulated correlation functions and the data in Fig. 4 is an overestimation of the height of the peak by the model, or an excessive value of R from the model, Eqs. (1) and (6), around $q = 20$ MeV/c. This can be attributed to the missing late-time emission of protons from a cascade of secondary decays, which is not modeled in pBUU. On the one hand, these contribute proton pairs that are widely spread out in the relative distance in their cm. On the other hand, when there, they lower the fraction of the proton-proton pairs emitted at short distances or $S(r)$ at short distances r . As a remedy, in the literature, the size of R has been adjusted by a factor of λ either matching the measured strength of the correlation around the $q = 20$ MeV/c peak [5] or making λ equal to the short-distance integral of S from data imaging [6, 29] still to be discussed here.

IV. IMAGING SOURCE THROUGH DEBLURRING

In optics, the blurring relation between a measured distribution, g , and an unknown distribution, \mathcal{G} , can be stated as [13, 15, 32]

$$g(t') = \int dt A(t', t) \mathcal{G}(t). \quad (11)$$

Here, $A(t', t)$ is the conditional probability that the quantity with an actual property t is attributed the property t' in a measurement. That probability is also known as the response function. The imaging task is to infer the true function \mathcal{G} , knowing g and A . That task may be achieved with the Richardson-Lucy (RL) algorithm discussed below. We may note that the relation (11) is of a form analogous to (1).

When the distributions are discretized, which happens naturally when photons contribute to individual pixels, the relation in (11) acquires a matrix form between the distribution arrays:

$$g_i = \sum_j A_{ij} \mathcal{G}_j. \quad (12)$$

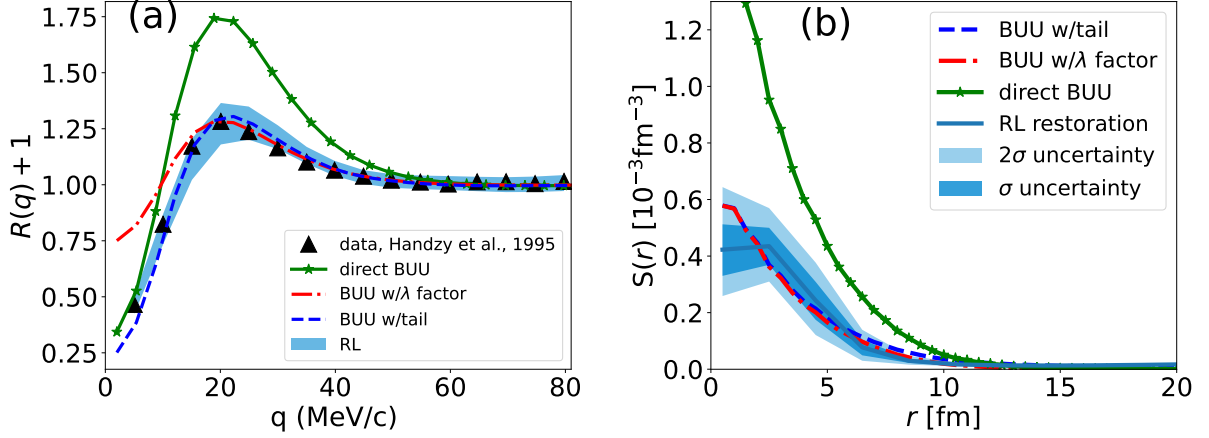


FIG. 5. Proton-proton correlation (a) and source (b) in central $^{36}\text{Ar} + ^{45}\text{Sc}$ collisions at 80 MeV/nucleon, within the total momentum range (200-400) MeV/c. The triangles in (a) represent the correlation data of Ref. [25]. The shaded regions in (b), with a central line, represent the results from deblurring the data in (a). The corresponding correlation results are indicated in (a). Finally, pBUU results are depicted in both panels in the direct version and with the addition of a tail and corresponding renormalization of the direct contribution.

We can see an analogous mathematical structure in Eqs. (1) and (11). Moreover, each of the quantities in (1) has a probabilistic interpretation, although only S is directly related to \mathcal{G} in (12). We will mainly rely on the mathematical analogy and attempt to use the RL method from optics to estimate S [14]. Further, in discussing the RL method, we will stick with the appropriate notation for the KP equation, assuming that the correlation function and the source are angle-averaged. In the future, the latter assumption may be lifted.

Specifically, in the present problem we consider the source range from $r = 0.5$ to 22 fm. We discretize the source S in that range into M even bins, so the source is approximated as

$$S(r) = \sum_{j=1}^M S_j w_j(r), \quad (13)$$

where w_j is the characteristic function associated with the j 'th bin. In the simplest case, that function is just

$$w_j(r) = \begin{cases} 1, & \text{if } r_{j-1/2} < r < r_{j+1/2}, \\ 0, & \text{otherwise.} \end{cases} \quad (14)$$

With the correlation function determined at momenta q_i , $i = 1, \dots, N$, the mapping of the correlation onto the optical blurring problem amounts to the obvious $C(q_i) \equiv C_i \leftrightarrow g_i$, $S(r_j) \equiv S_j \leftrightarrow g_j$, and

$$K_{ij} \equiv 4\pi \int_{r_{j-1/2}}^{r_{j+1/2}} dr r^2 K(q, r) \leftrightarrow A_{ij}.$$

In both cases, the kernels, K_{ij} and A_{ij} , respectively, are nonnegative. The number of bins we choose for the source function generally does not exceed the number of data points in the correlation function, that is, $M \leq N$. The

correlation function shown in Fig. 4 and 5 (a) has $N=16$ data points and the source function is assumed to be decomposed into $M=11$ bins in Eq. 13. This choice determines the resolution of the source with a bin size $\Delta r = 2$ fm, obtained from r_{\max}/M .

The RL algorithm determines the distribution S when C and K are known. To arrive at the RL strategy, a backward relation between C and S is invoked, which involves a conditional probability \tilde{K} that is complementary to K . The fulfillment of a Bayesian relation involving K , \tilde{K} , and S is arrived at through iterations [29, 33]

$$S_j^{(n+1)} = \mathcal{M}_j^{(n)} S_j^{(n)}, \quad (15)$$

where

$$\mathcal{M}_j^{(n)} = \frac{\sum_i \alpha_i \frac{C_i}{C_i^{(n)}} K_{ij}}{\sum_{i'} \alpha_{i'} K_{i'j}}. \quad (16)$$

Here, \mathbf{n} is the iteration index, $\mathcal{M}_j^{(n)}$ is an amplification factor, and $C^{(n)}$ is prediction for the observation at \mathbf{n}^{th} iteration:

$$C_i^{(n)} = \sum_j K_{ij} S_j^{(n)}. \quad (17)$$

The weights α in (16) can serve as importance factors and may be chosen as inverse errors or weights that amplify the importance of the low relative momentum region where C can really tell about S .

This paper uses the RL algorithm to extract the proton-proton source function from the experimental correlations reported by Verde *et al.* [5]. In Fig. 5(a), we show the proton-proton correlation functions for the reaction $^{36}\text{Ar} + ^{45}\text{Sc}$ at 80 MeV / nucleon and a total pair momentum range of 200–400 MeV/c. The deblurred source

functions obtained are displayed in panel (b). The RL algorithm described in Eq. (16) provides the source profiles shown as shaded blue bands in panel (b). These source functions are then used in the KP equation, Eq. (10), to obtain the deblurred correlation function shown as the corresponding blue-shaded band in panel (a).

We employ an error resampling technique to quantify the uncertainties in these reconstructed source functions and deblurred correlations (see Ref. [13] for details). The bands shown represent the uncertainties obtained by performing error resampling on the measured correlation functions. The dark and light blue bands of the source functions in panel (b) correspond to the σ and 2σ intervals, respectively, and the solid blue line denotes the mean source function of 1000 samples. Ideally, measured experimental errors would be used for resampling; however, the data extracted from [5] lack detailed error information. Consequently, the uncertainties are approximated using a Gaussian distribution, $\mathcal{N}(0, \sigma)$, with $\sigma = 0.045$ for relative momenta $q \geq 15$ MeV/c and $\sigma = 0.1$ for $q \leq 15$ MeV/c, where larger uncertainties are expected. Additionally, the blue band in the correlation functions in panel (a) represents the 2σ uncertainty associated with the source function.

Also, it is important to mention that the measured correlations are affected by detector resolutions, particularly at low values of q . To account for these resolution effects in our calculation, the proton-proton kernel is smeared in q by folding the original kernel with a Gaussian in q of width $\sigma_q = 2.8$ MeV/c [14] and references within.

In the context of statistical uncertainties introducing short-wavelength variations in the input data, discussing a possible instability in the RL and other inversion methods for integral relations, such as the KP equation, is essential. A forward relation, such as the KP relation, tends to suppress the impact of short-wavelength components, and a reverse relation tends to amplify them, including those spuriously induced by finite measurement statistics, raising the potential for an instability. Generally, the positive definiteness of the restored source S stabilizes the inversion. In addition, we employ the Total Variation regularization, as described in our previous studies, see Refs.[13–15], with a small regularization factor of 0.0005. In particular, recent work [23] has shown that maximum entropy regularization is also effective in extracting the proton-proton source function from experimental correlations using the RL algorithm.

V. PBUU STUDY OF THE TWO-PROTON EMITTING SOURCE

We now compare the source function, obtained with the RL algorithm from the measured correlation function shown again in Fig. 5(a), with the predictions of the pBUU simulations. The solid red line in Fig. 5(b) shows the source function, $S^{BUU}(r)$, from combining Eq. (8)

with pBUU simulations. Since the differences between the sources for soft and stiff EOSs, with and without momentum dependence, are minimal, as shown in Fig. 3, we focus on an exemplary stiff and momentum-independent EOS here. We also plot in Fig. 5(a), the correlation function obtained by inserting this pBUU source into the KP equation, using Eq. (7), again as a solid red line.

To correct for the apparent overestimate of the source strength at short relative distances, the pBUU source is next renormalized by a λ factor to obtain the correlation strength at $q \sim 20$ MeV/c and above right, similarly to the procedure used in [5]. The resulting renormalized pBUU source is shown as a dot-dashed green line in Fig. 5(b). After adjustment of the pBUU source strength, its shape generally agrees with the source imaged from data up to distances $r \sim 10$ fm and so does its integral, close to λ over these distances. The correlation for the renormalized source is shown as a green dot-dashed line in Fig. 5(a) and it is apparent that it misses the data for $q < 18$ MeV/c, the region that can be attributed to pairs where at least one member is emitted through slower emission mechanisms generally missing from a BUU reaction description.

Although finding that a transport model can describe the fast portion of the emission source is satisfying and comparison to data can inform on the fraction of fast pp pairs, we put forward here a new approach where we quantify the tail missing from a BUU source, within the distances that data probe. Specifically, we combine the transport source with a phenomenological addition, suppressed at short distances where the transport model should work, and picking up and gradually falling off at large distances [34]:

$$S(r) = \lambda S^{BUU}(r) + \frac{1 - \lambda}{96\pi B^5} r^2 \exp(-r/B), \quad (18)$$

The source addition, incorporating a fall-off parameter B , is normalized to integrate to $(1 - \lambda)$. The whole source (18) integrates to 1.

We alternatively determine the optimal parameters λ and B by fitting the source (18) to the source restored from the data or the correlation obtained from the source (18) to the measured correlation [5]. The results are similar in the two cases. In Fig. 5 we show the source (18) and associated correlation for $\lambda = 0.38$ and $B = 4.0$ fm. It can be seen in panel (a) that the data description is successful. Additional details on the tail-shaped theoretical source are provided in Fig. 6. The tail component is shown separately, and the inset magnifies the theoretical sources at large distances.

The dependence of the strength, λ , and the spatial extent, B , on the beam energy and the total momentum of the proton pairs may provide important information on the mechanisms of proton emission and the impact of long-lived secondary decays in fragmentation processes. However, this analysis is not easy to perform with the present set of data- more stringent gates on the impact parameter and the rapidity of the detected particles may

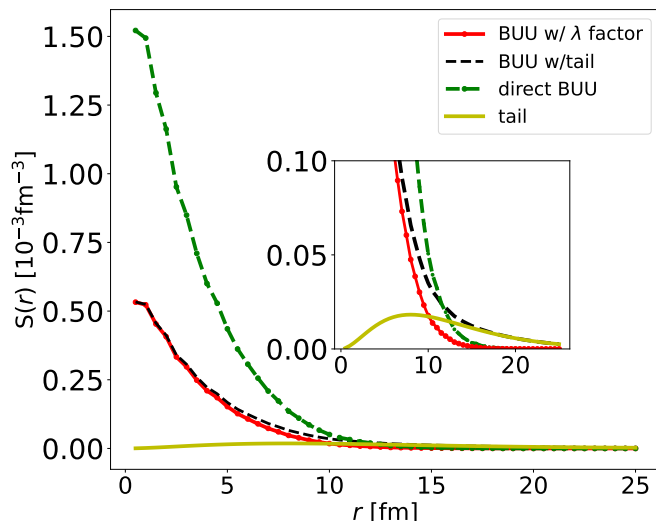


FIG. 6. Theoretical pp source function in the $^{36}\text{Ar} + ^{45}\text{Sc}$ reaction at beam energy of 80 MeV/nucleon and impact parameter of $b = 1.9$ fm. The green dash-dot line represents the source function obtained directly from pBUU. The red solid line superposed with dots represents the pBUU source multiplied by the $\lambda = 0.38$ factor. The blue dashed line represents the source function of Eq. (18), combining the reduced pBUU outcome and a tail. The yellow solid line shows the tail function separated, i.e., the second term of Eq. (18) for $B = 4$ fm. The inset shows details in the fall-off of the theoretical distributions.

be needed to isolate emitting regions better during collisions. This task is beyond the scope of this article, but it represents an important opportunity for the future exploration of other reaction systems.

VI. SUMMARY AND OUTLOOK

In this work, we have confronted the proton-proton correlation functions measured in $^{36}\text{Ar} + ^{45}\text{Sc}$ reaction at $E/A=80$ MeV with predictions of the pBUU transport model. The shape of pBUU correlation functions for this system shows a very weak sensitivity to the stiffness of the EoS and momentum-dependent interactions. As previously observed in the literature, the absence of sec-

ondary decay modeling in transport models results in difficulties reproducing the experimental correlation function. We used the deblurring imaging technique to invert the KP equation and determine a source to study the effects of long-lived emissions better. Then, this source shape was compared with pBUU-calculated sources and used to assess the secondary-decay contributions to the source more quantitatively than in the past. A renormalization of a transport-model source function, employed previously in the literature, while forcing to fit the height of the peak at 20 MeV/c in the correlation function, cannot address the correlation-function shape at small relative momenta. Instead, adding an analytical tail function to the pBUU emitting source and fitting its two free parameters to the deblurred source, leads to a two-proton source function that adequately describes the experimental correlation function at small q -values and the peak height. Given that only a few data points may be obtained in measurements at low relative q , the falloff scale for the source tail at intermediate distances may be all that can be firmly established. However, if measurement resolution progresses, more may be learned from imaging and/or expanding source parameterization. From the side of transport models, the simple parametrization introduced for the source function allows for quantifying the shortcomings of a transport model, such as pBUU, that the specific or other models may eventually need to breach.

In perspective, it would be important to study directional correlation functions by expanding the pBUU source functions into angular components [35]. Especially, using the quadrupole components of the source function may help us gaining more quantitative information about the distribution of emissions from second decays. In addition, a systematic Femtoscopy analysis, extended to various heavy-ion collision systems over ranges of masses and beam energy, may contribute to improve transport models providing possible useful probes of the nuclear equation of states.

This work was supported by the U.S. Department of Energy through Los Alamos National Laboratory. Triad National Security, LLC operates Los Alamos National Laboratory for the National Nuclear Security Administration of the U.S. Department of Energy (Contract No. 89233218CNA000001). The authors acknowledge the support from the US Department of Energy Office of Science under Grant No. DE-SC0019209.

-
- [1] H. Wolter, M. Colonna, D. Cozma, P. Danielewicz, C. M. Ko, R. Kumar, A. Ono, M. B. Tsang, J. Xu, Y.-X. Zhang, et al., *Progress in Particle and Nuclear Physics* **125**, 103962 (2022), ISSN 0146-6410, URL <https://www.sciencedirect.com/science/article/pii/S0146641022000230>.
 - [2] P. Danielewicz, *Nuclear Physics A* **673**, 375 (2000), ISSN 0375-9474, URL <https://www.sciencedirect.com/science/article/pii/S037594740000083X>.

- [3] A. Ono and H. Horiuchi, *Progress in Particle and Nuclear Physics* **53**, 501 (2004), ISSN 0146-6410, URL <https://www.sciencedirect.com/science/article/pii/S0146641004000936>.
- [4] A. Sorensen, K. Agarwal, K. W. Brown, Z. Chajewski, P. Danielewicz, C. Drischler, S. Gandolfi, J. W. Holt, M. Kaminski, C.-M. Ko, et al., *Progress in Particle*

- and Nuclear Physics **134**, 104080 (2024), ISSN 0146-6410, URL <https://www.sciencedirect.com/science/article/pii/S0146641023000613>.
- [5] G. Verde, P. Danielewicz, D. A. Brown, W. G. Lynch, C. K. Gelbke, and M. B. Tsang, Phys. Rev. C **67**, 034606 (2003), URL <https://link.aps.org/doi/10.1103/PhysRevC.67.034606>.
 - [6] G. Verde, D. A. Brown, P. Danielewicz, C. K. Gelbke, W. G. Lynch, and M. B. Tsang, Physical Review C **65**, 054609 (2002), publisher: American Physical Society, URL <https://link.aps.org/doi/10.1103/PhysRevC.65.054609>.
 - [7] P. Danielewicz and G. Bertsch, Nuclear Physics A **533**, 712 (1991), ISSN 0375-9474, URL <http://www.sciencedirect.com/science/article/pii/037594749190541D>.
 - [8] G. Bertsch and S. Das Gupta, Physics Reports **160**, 189 (1988), ISSN 0370-1573, URL <https://www.sciencedirect.com/science/article/pii/0370157388901706>.
 - [9] W. Bauer, Progress in Particle and Nuclear Physics **30**, 45 (1993).
 - [10] S. E. Koonin, Physics Letters B **70**, 43 (1977).
 - [11] S. Pratt, Physical Review Letters **53**, 1219 (1984).
 - [12] D. A. Brown and P. Danielewicz, Physics Letters B **398**, 252 (1997).
 - [13] P. Nzabahimana, T. Redpath, T. Baumann, P. Danielewicz, P. Giuliani, and P. Guèye, Phys. Rev. C **107**, 064315 (2023), URL <https://link.aps.org/doi/10.1103/PhysRevC.107.064315>.
 - [14] P. Nzabahimana and P. Danielewicz, Physics Letters B **846**, 138247 (2023), ISSN 0370-2693, URL <https://www.sciencedirect.com/science/article/pii/S0370269323005816>.
 - [15] P. Danielewicz and M. Kurata-Nishimura, Phys. Rev. C **105**, 034608 (2022).
 - [16] L.-W. Chen, V. Greco, C. M. Ko, and B.-A. Li, Phys. Rev. Lett. **90**, 162701 (2003), URL <https://link.aps.org/doi/10.1103/PhysRevLett.90.162701>.
 - [17] D. A. Brown and P. Danielewicz, Physics Letters B **398**, 252 (1997), ISSN 0370-2693, URL <https://www.sciencedirect.com/science/article/pii/S0370269397002517>.
 - [18] P. Danielewicz and P. Schuck, Physics Letters B **274**, 268 (1992), ISSN 0370-2693, URL <http://www.sciencedirect.com/science/article/pii/037026939291985I>.
 - [19] G. Verde, A. Chbihi, R. Ghetti, and J. Helgesson, The European Physical Journal A-Hadrons and Nuclei **30**, 81 (2006).
 - [20] G. Goldhaber, S. Goldhaber, W. Lee, and A. Pais, Physical Review **120**, 300 (1960), publisher: American Physical Society, URL <https://link.aps.org/doi/10.1103/PhysRev.120.300>.
 - [21] D. H. Boal and J. C. Shillcock, Phys. Rev. C **33**, 549 (1986), URL <https://link.aps.org/doi/10.1103/PhysRevC.33.549>.
 - [22] D. H. Boal, C.-K. Gelbke, and B. K. Jennings, Rev. Mod. Phys. **62**, 553 (1990), URL <https://link.aps.org/doi/10.1103/RevModPhys.62.553>.
 - [23] C.-K. Tam, Z. Chajecski, P. Danielewicz, and P. Nzabahimana, arXiv preprint arXiv:2502.09478 (2025), URL <https://arxiv.org/abs/2502.09478>.
 - [24] J. Xu, Z. Qin, R. Zou, D. Si, S. Xiao, B. Tian, Y. Wang, and Z. Xiao, Chinese Physics Letters (2025), URL <http://iopscience.iop.org/article/10.1088/0256-307X/42/3/031401>.
 - [25] D. O. Handzy, W. Bauer, F. C. Daffin, S. J. Gaff, C. K. Gelbke, T. Glasmacher, E. Gualtieri, S. Hannuschke, M. J. Huang, G. J. Kunde, et al., Phys. Rev. Lett. **75**, 2916 (1995), URL <https://link.aps.org/doi/10.1103/PhysRevLett.75.2916>.
 - [26] H. Lin and P. Danielewicz, Phys. Rev. C **99**, 024612 (2019), URL <https://link.aps.org/doi/10.1103/PhysRevC.99.024612>.
 - [27] H. M. Xu, W. G. Lynch, P. Danielewicz, and G. F. Bertsch, **65**, 843 (1990), publisher: American Physical Society, URL <https://link.aps.org/doi/10.1103/PhysRevLett.65.843>.
 - [28] D. H. Boal, C.-K. Gelbke, and B. K. Jennings, Rev. Mod. Phys. **62**, 553 (1990), URL <https://link.aps.org/doi/10.1103/RevModPhys.62.553>.
 - [29] P. Nzabahimana, Ph.D. thesis, Michigan State University (2023).
 - [30] N. Colonna, D. R. Bowman, L. Celano, G. D'Erasmus, E. M. Fiore, L. Fiore, A. Pantaleo, V. Paticchio, G. Tagliente, and S. Pratt, Phys. Rev. Lett. **75**, 4190 (1995), URL <https://link.aps.org/doi/10.1103/PhysRevLett.75.4190>.
 - [31] D. A. Brown and P. Danielewicz, Physical Review C **57**, 2474 (1998).
 - [32] G. Zech, Nuclear Instruments and Methods in Physics Research Section A: Accelerators, Spectrometers, Detectors and Associated Equipment **716**, 1 (2013), ISSN 0168-9002, URL <https://www.sciencedirect.com/science/article/pii/S0168900213003148>.
 - [33] W. H. Richardson, JoSA **62**, 55 (1972).
 - [34] P. Nzabahimana, P. Danielewicz, and G. Verde, IL Nuovo Cimento **100**, 48 (2025).
 - [35] P. Danielewicz and S. Pratt, Phys. Rev. C **75**, 034907 (2007), URL <https://link.aps.org/doi/10.1103/PhysRevC.75.034907>.